PdAu membranes supported on top of vacuum-assisted ZrO₂-modified porous stainless steel substrates

Ana Tarditi, Camila Gerboni, Laura Cornaglia*

Instituto de Investigaciones en Catálisis y Petroquímica (FIQ, UNL-CONICET), Santiago del Estero 2829, 3000 Santa Fe, Argentina

ARTICLE INFO

ABSTRACT

To enable the formation of defect-free PdAu composites by electroless plating, the vacuum-assisted ZrO₂-modified method was optimized on top of porous stainless steel disks. Both the ZrO₂-modified supports and the PdAu synthesized membranes were characterized by XRD (X-ray diffraction), SEM (scanning electron microscopy), EDS (energy dispersive X-ray analysis) and XPS (X-ray photoelectron spectroscopy). SEM cross-section results showed that dense, continuous, defect-free PdAu films were deposited on top of the ZrO₂-modified PSS disks, and the EDS data indicated that no significant concentration gradient was present on the thickness. At 400 °C and 100 kPa, the pure hydrogen permeation flux for a 10 μm thick PdAu membrane was about 0.14 mol s^{-1} m^{-2} and the H₂/N₂ ideal selectivity was higher than 10,000.

1. Introduction

Palladium membranes have been proposed as an efficient technology to be applied on hydrogen production and purification processes. They can be integrated into a hydrogen production reactor enabling a more compact and highly efficient process design. The use of dense palladium-based membranes appears as a potential route to hydrogen separation from the mixture stream due to their high perm-selectivity to hydrogen. However, their actual implementation is limited by their low mechanical stability and their high costs. Composite membranes, formed by a thin palladium layer on top of a porous substrate (ceramic, glass, or stainless steel) constitute an economic option to overcome these limitations. Commercially available supports with smooth surface and small pore sizes allow the synthesis of thinner Pd layers on top of them; however, they are expensive as they are composed of several layers with decreasing pore size.

Porous stainless steel (PSS) are promising substrates due to their good mechanical strength, operation at high temperature and simplicity of module construction [1]. Nevertheless, the pore size and roughness of these supports impair the fabrication of a thin defect-free Pd layer on top of them. To overcome this problem, the deposition of an intermediate layer between the PSS substrates and the Pd layer is usually implemented. A wide variety of materials have been used as support modifiers such

as Al₂O₃ [2], SiO₂ [3], CeO₂ [4] and WO₃ [5]. Zeolites such as NaA [6] have also been employed as successfully intermediate barriers for Pd-based membranes. From a different approach, the in situ formation of an iron and cromium oxide layer, by heating the stainless steel in air flux at several temperatures, was reported by Ma et al. [7]. Alternatively, zirconia is considered to be an excellent material to modify the PSS surface due to both its good chemical stability at high temperatures and its thermal expansion coefficient comparable to that of stainless steel. Way and coworkers [8], using commercial available yttria-stabilized zirconia (YSZ) PSS supports, reported the synthesis and evaluation of PdAg and PdAu membranes by electroless plating of a thickness between 1 and 7 μm. Recently, Sanz et al. [9] reported the synthesis of a Pd membrane on top of an yttria-stabilized zirconia modified porous stainless steel tubular support. The YSZ interphase of about 50 μm thickness was prepared by Atmospheric Plasma Spraying and the palladium membrane by electroless deposition. They reported that a thickness of 27.7 μm of Pd layer was necessary to achieve a dense and defect-free membrane.

In addition to the above-mentioned issue, pure palladium undergoes a phase transition when exposed to hydrogen at temperatures below 300 °C, causing irreversible embrittlement in the Pd film. Also, Pd films can be irreversibly poisoned by sulfur compounds and other feedstock poisons which produce inhibition of the H₂ transport in the membrane. The presence of other metals as silver, ruthenium, copper and gold, at specific concentrations, also enhances the hydrogen permeation flux with no negative effects on its selectivity [10]. PdAu membranes are interesting to be applied in a hydrogen production reactor not only because they do not exhibit hydrogen embrittlement even at

* Corresponding author. Tel.: +54 342 4536861; fax: +54 342 4571162.
E-mail addresses: lmcornag@fiq.unl.edu.ar,
lmcornag@fiqus.unl.edu.ar (L. Cornaglia).

room temperature, but also because PdAu alloys are more resistant to H_2S poisoning. Way et al. [10] observed a 38% permeance decline on a $Pd_{85}Au_{15}$ membrane in the presence of 5 ppm H_2S at 400 °C. On the other hand, Ma and coworkers [11] found that a PdAu membrane with a 8 wt% Au was resistant to bulk sulfidation upon exposure to 54.8 ppm H_2S/H_2 stream in the temperature range between 350 and 500 °C. In addition, self-supported alloys of 0–10 atomic% Au were shown to have higher hydrogen permeabilities than pure Pd [12].

The objective of the present work was to optimize the vacuum-assisted ZrO_2 dip-coating technique in order to reduce the thickness required to obtain defect-free PdAu composite membranes. The samples were synthesized on top of porous stainless steel disks of both 0.2 and 0.1 μm grade. Surface and bulk composition, structure and morphology of both the ZrO_2-modified support and the PdAu membranes were studied. The H_2 permeation properties of the composite membranes were evaluated as a function of temperature and pressure.

2. Experimental

Vacuum-assisted ZrO_2 modification. Porous stainless steel disks (PSSD, 1.27 cm in diameter) 0.1 and 0.2 μm grade were used as supports of the composite PdAu alloy membranes. The supports were purchased from Mott Metallurgical Corporation. Prior to any plating experiment, they were cleaned in a basic solution consisting of 0.12 M $Na_3PO_4 \cdot 12H_2O$, 0.6 M Na_2CO_3 and 1.12 M NaOH using the procedure reported by Ma and co-workers. [1]. After that, the substrates were oxidized at 500 °C for 12 h. In order to avoid inter-metallic diffusion and modify both the pore size and the surface roughness, the supports were modified with zirconium by means of the dip coating vacuum-assisted method. For the zirconium dip-coating solution polyvinyl alcohol (PVA) was added to a colloidal ZrO_2 suspension (Nyacol Acetate Stabilized 20 wt%, particle size between 5 and 10 nm) to reach a composition of 0.025 M ZrO_2 and 2 wt% PVA. For the few first depositions, the support was introduced vertically into the dip coating solution without vacuum and the vaccum-assisted method was used in the last deposition stages. Vacuum was used to better introduce the ZrO_2 suspension into the substrates pores and modify the pore size. After each coating, the support was dried at room temperature for 1 h and the following dipping was performed. Finally, when a deposition cycle (three ZrO_2 coatings) was carried out, the samples were calcined at 500 °C for 3 h. The temperature of the reactor was increased from room temperature up to 500 °C with a heating rate of 0.5 °C min^{-1} in air flow. Five deposition-calcination cycles were perfomed for each sample.

In order to analyze the effect of the intermediate calcinations and to optimize the support modification procedure, two different samples were prepared. One sample was calcined up to 500 °C in air during 5 h after the first deposition cycle. Then, the sample was coated with a second ZrO_2 deposition cycle and finally calcined at 500 °C in air during 5 h. The other sample was prepared in the same way with the only difference that it was not subjected to an intermediate calcination between the two deposition cycles.

Membrane preparation. Solutions for activation were prepared using tin(II) chloride dehydrate and palladium(II) chloride. The chemical composition of the activation was $SnCl_2$ 1 g L^{-1}, pH 2 and $PdCl_2$ 0.1 g L^{-1}, pH 2. The electroless plating technique (ELP) was used to coat the support with a continuous metallic film. For the PdAu membranes, palladium and gold were deposited by sequential electroless deposition using the bath compositions shown in Table 1. First, palladium was deposited in two steps for 60 min each at 50 °C, followed by an Au deposition of 20 min

Table 1
Chemical composition of the Pd, Au electroless plating solutions and plating conditions.

Components of plating solution	Pd bath	Au bath
$PdCl_2$ (g/l)	3.6	–
NH_4OH (ml/l)	650	–
$Na_2EDTA \cdot 2H_2O$ (g/l)	67	–
N_2H_4 1 M (ml/l)	10	–
$AuCl_3 \cdot HCl \cdot 4H_2O$ (g/l)	–	4.15
NaOH (g/l)	–	0.18
Na_2SO_3 (mol/l)	–	0.17
$Na_2S_2O_3 \cdot 5H_2O$ (mol/l)	–	0.15
L-$C_6H_8O_6$ (mol/l)	–	0.34
pH	11	11
Temperature (°C)	50	60

at 60 °C. After the Pd and Au depositions, the samples were rinsed with water and dried at 120 °C overnight. The synthesis procedure was repeated until the composite membrane became impermeable to N_2 at room temperature and at a pressure difference of 10 kPa. The gas-tightness of the membranes was confirmed by zero measurable nitrogen permeation flux at room temperature, which was corroborated by means of an Ar sweep gas flow with a differential pressure of 10 kPa, analyzed by a mass spectrometer. Then, the samples were heated up to 500 °C in a H_2 atmosphere in order to promote metallic inter-diffusion and alloy formation. The temperature of the reactor was increased from room temperature up to 500 °C with a heating rate of 0.5 °C min^{-1} in nitrogen flow and then, the annealing process was conducted in hydrogen atmosphere. The plating surface area per volume of bath was kept at 225 cm^2 L^{-1}. By the mass gain after each deposition cycle, we were able to estimate the thickness of both Pd and Au layers and calculate the gold composition. The final film thickness was estimated from the weight gain and checked by SEM.

For the sake of comparison, an Al_2O_3-modified PSSD support was prepared using the previously reported dip-coating method [13]. The modification was performed using three different Al_2O_3 slurries prepared with powers of two grain sizes, 1 μm and 50 nm and a mixture of both. During the dip-coating, the aluminum oxide was forced to penetrate inside the porous of the substrate by means of a vacuum system. After the immersion in each slurry, a short Pd electroless deposition was performed as described elsewhere [13].

2.1. Membrane characterization

2.1.1. X-ray diffraction
The structural properties of the membranes were determined by X-ray diffraction. The XRD patterns of the samples were obtained with an XD-D1 Shimadzu instrument, using Cu K_α ($\lambda = 1.542$ Å) radiation at 30 kV and 40 mA. The scan rate was 1° min^{-1} in the $2\theta = 15$–90° range.

2.1.2. Scanning electron microscopy and energy-dispersive X-ray analysis
The top surface and cross-sectional images of the samples were obtained using a JEOL scanning electron microscope; model JSM-35 C, equipped with an energy dispersive analytical system (EDAX) used to determine the bulk atomic composition of the membranes.

2.1.3. X-ray photoelectron spectroscopy
XPS analyses were performed in a multi-technique system (SPECS) equipped with an Al-monochromatic X-ray source, and a

hemispherical PHOIBOS 150 analyzer operating in the fixed analyzer transmission (FAT) mode. The spectra were obtained using a monochromatic Al K_α radiation ($h\upsilon = 1486.6$ eV) operated at 300 W and 14 kV. The pass energy for the element scan was 30 eV. The working pressure in the analyzing chamber was less than 5×10^{-10} kPa. The XPS analyses were performed on the annealing samples and after different treatments in the main chamber. Before introducing the samples into the main chamber of the spectrometer, they were heated up in H_2 5%/Ar mixture at 400 °C in the load-lock chamber. The spectra of Pd 3d, Pd 3p, O 1s, C 1s, Au 4f and their corresponding Auger peaks plus the valence band regions were recorded for the PdAu samples and the Zr 3d, Fe 3p, Ni 2p and Cr 2p regions for the the oxidized and the ZrO_2-modified supports. The data treatment was performed with the Casa XPS program (Casa Software Ltd, UK). The peak areas were determined by integration employing a Shirley-type background. Peaks were considered to be a mixture of Gaussian and Lorentzian functions. For the quantification of the elements, we used the sensitivity factors provided by the manufacturer.

2.2. Permeation measurements

Single gas permeation experiments were conducted using the permeation module reported elsewhere [14]. High-purity hydrogen and nitrogen were used for the experiments. The permeator was placed in an electric furnace and heated to the desired temperatures. A thermocouple within the membrane monitored and controlled the temperature during the experiments. All the gases were fed to the permeator using calibrated mass-flow controllers. The Pd alloy side of the membrane was flushed with feed gases, while the other side was flushed with N_2 as sweep gas (permeate side) during the heat procedure. No sweep gas was used on the permeate side during the single-gas permeation experiments. Pressure differences across the membranes were controlled using a back-pressure regulator. The upstream was varied while keeping the downstream pressure constant at 100 kPa. The gas permeation flow rates of either H_2 or N_2 were measured using two bubble flow meters at room temperature and

pressure. However, an Ar sweep gas flow was employed with a differential pressure of 100 kPa, to check the N_2 leak with a mass spectrometer. The permeation areas were 1.2 cm². All temperature changes were carried out in N_2 atmosphere. The nomenclature adopted for the membranes was PdAuXY, where X refers to material used as modifier of the PSS substrate (Al_2O_3 or ZrO_2), and Y to grade of the support (0.1 or 0.2).

3. Results and discussion

3.1. ZrO₂ support modification

In order to avoid inter-metallic diffusion and decrease metallic film thickness, vacuum-assisted dip-coating of colloidal ZrO_2 was performed on top of porous stainless steel disks before metallic electroless deposition. As it is well known, the surface morphology of the commercial available porous stainless steel supports presents pores of a size between 2 and 10 µm in diameter. For that reason, the use of a modified support is needed in order to obtain a continuous defect-free palladium alloy layer on top of them [15].

In order to optimize the ZrO_2 deposition on top of both 0.2 and 0.1 µm grade supports, two different PSS0.2 disks were coated with two deposition cycles. One of them, was calcined up to 500 °C in air during 5 h after the first deposition cycle. The other sample was prepared without the intermediate calcination between the two deposition cycles. The sample with an intermediate calcination presented a higher weight gain (4.2 ± 40.3 mg) than the other one. Besides, when the top surface of the samples was observed by SEM, it was possible to notice that this sample exhibited a more homogeneous and compact coverage, filling the pores of the substrate (Fig. 1B and D). Note that the sample without intermediate calcination had a lower amount of ZrO_2 inside the pores (Fig. 1A and C). The calcinations after each deposition cycle allowed the ZrO_2 particles to have a better anchorage to the support, improving the adherence of the coating.
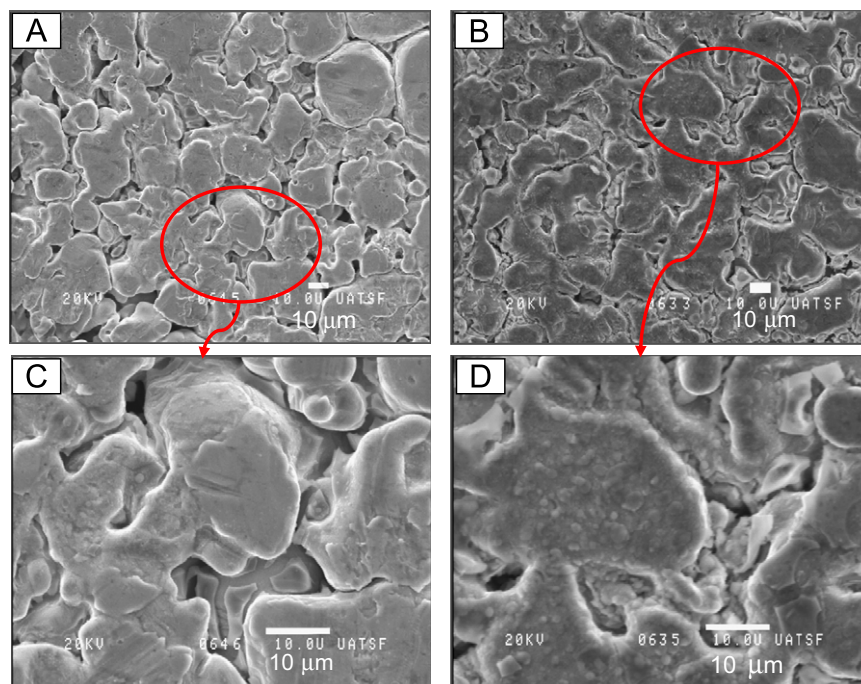

Fig. 1. Effect of the intermediate calcination on the ZrO_2 deposition. SEM top view of the 0.2 µm support with two deposition cycles followed by calcination: (A) and (C) without intermediate calcination; (B) and (D) with intermediate calcination.
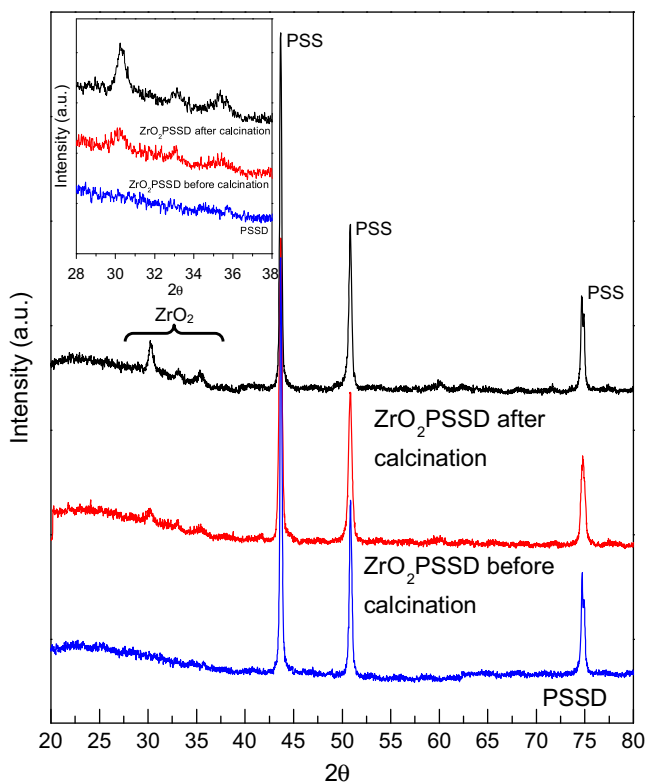
Fig. 2. X-ray diffraction patterns of the 0.2 µm support before and after calcination of the first zirconia deposition cycle.

When the sample was exposed to air at high temperature after the first deposition cycle, more intense peaks with respect to those of the non-calcined sample were observed by XRD (Fig. 2). The XRD data showed that the film crystallized into a tetragonal phase, in agreement with the data reported by Chang et al. [16]. The main peaks of the tetragonal phase could be seen at 30.2° and 35°. Besides, three peaks at 43.6°, 50.7° and 74.8° assigned to the γ-phase of the stainless steel substrate could be observed. No peak assigned to the ZrO_2 monoclinic phase was observed in the XRD profile. Chang et al. [16] reported that for a ZrO_2 film exposed to air between 400 and 500 °C, a tetragonal ZrO_2 phase was stable, showing a phase transformation (from tetragonal to monoclinic) at temperatures higher than 550 °C [16]. Using a sol-gel dip coating method, Gao et al. [17] reported the formation of a ZrO_2 thin layer of about 2 µm on top of porous stainless steel disks. From XRD measurements after treatment in H_2 flow at 500 °C, they claimed that the ZrO_2 layer crystallized in a cubic zirconia phase. However, as reported in the literature, due to the lattice parameters associated with the cubic and tetragonal ZrO_2 phases, it is difficult to differentiate a phase from another by XRD only.

Figs. 3 and 4 show the characteristic surface morphology of the ZrO_2-modified PSS substrates after all deposition-calcination cycles. The SEM images of the original PSS substrate are also shown for comparison. It appears that after coating, the surface becomes smoother and a complete coverage of the porous is observed in both the 0.2 and 0.1 grade supports (Figs. 3 and 4). This effect is even more marked in the case of the 0.1 µm porous support (Fig. 4), after the same number of deposition-calcination cycles. When the surface of the original supports is examined, it is possible to observe that the pore size openings are higher in the 0.2 µm than in the 0.1 µm grade support (Figs. 3 and 4). In the case of the 0.1 µm grade substrate, a better coverage of the support could be reached maybe due to the smaller pore size exposure on the surface. As previously reported, both the pore

size and porosity of the substrate may affect the palladium layer thickness and perm-selectivity properties of palladium membranes prepared by electroless deposition technique [18].

From the SEM observation, it was possible to observe that the use of a vacuum-assisted ZrO_2-coating allowed us to obtain a more compact and resistant ZrO_2 layer on top of the porous stainless steel support. ZrO_2 penetrated into the pore system filling the pores, which improved the adhesion of the membrane to the substrate. A thin layer of ZrO_2 was obtained on top of the support surface.

The XPS surface atomic composition of the oxidized and ZrO_2-modified porous stainless steel substrates are reported in Table 2. Note that the support presents a surface atomic composition of Fe 20.9%, Cr 12.3% and O 66.8%. In addition, a contribution of C and O due to contamination could be observed on the surface. As shown in Table 2, the binding energy of the Fe $2p_{3/2}$ and Cr $2p_{3/2}$ core levels, 710.1 and 577.1 eV are assigned to Fe_2O_3 and Cr_2O_3, respectively. In the case of the ZrO_2-modified support, the Zr $3d_{5/2}$ spectrum shows a photoelectron emission at 182.2 eV typical of the ZrO_2 [19] and another peak at 530.4 eV assigned to O 1s. Besides, some C from contamination could be seen on the spectra. Neither Fe nor Cr was detected on the surface of the modified support. It indicates that a continuous thin layer of ZrO_2 has been formed on top of the PSS support. Furthermore, no migration of the substrate components to the ZrO_2 layer takes place under the calcination procedure.

3.2. Characterization of $PdAuZrO_2$ membranes

In order to evaluate the effectiveness of the vacuum-assisted ZrO_2-modified method, several PdAu membranes were synthesized on top of previously modified substrates. The performance of the membranes was evaluated by means of single component hydrogen permeation experiments and the H_2/N_2 ideal selectivity was determined. All membranes showed a Au composition of about 8–9% determined by EDS measurements (Tables 3 and 4).

Fig. 5 exhibits the XRD patterns of the $PdAuZrO_2$0.2 membrane after the metallic deposition, and that of the annealing at 500 °C during 120 h and subsequent hydrogen permeation experiments. The as-prepared sample yielded the expected Pd and Au diffraction peaks. After annealing and subsequent hydrogen permeation experiments, the peaks of Pd and Au vanished and it was possible to observe the formation of the FCC phase of the PdAu binary alloy. As it is known, Pd and Au form a continuous solid solution with a FCC phase at all atomic compositions [20]. It is worth mentioning that in the XRD patterns, no reflection peaks from Fe, Cr and Ni were observed. All PdAu alloy membranes exhibited the same XRD diffraction patterns as the $PdAuZrO_2$0.2. Using a 3 µm thick electroless plated sample, Shi et al. [20] reported that the formation of a homogeneous PdAu alloy was very slow at 500 °C. To corroborate the alloy formation after 120 h at 500 °C, we used a reference sample prepared on top of non-porous stainless steel supports. After annealing during 120 h at 500 °C in H_2 atmosphere, the same XRD pattern as the $PdAuZrO_2$0.2 membrane was observed. This fact suggested that the hydrogen permeation experiments did not produce any change on the crystalline structure of the composite membranes. From the XRD data, the lattice constant obtained for the PdAu composite membranes was 3.905 Å, which gives an Au composition of about 8%.

For the sake of comparison, a $PdAuAl_2O_3$0.2 membrane was also prepared on top of an Al_2O_3-modified PSSD support. If the SEM top view of $PdAuZrO_2$0.2 and $PdAuAl_2O_3$0.2 are compared (Fig. 6), it is possible to observe that both membranes exhibit a uniform coverage of the PdAu alloy on the support with more notorious grain boundaries in the case of the Al_2O_3-modified support (Fig. 6 A and B). It appears that the surface of the
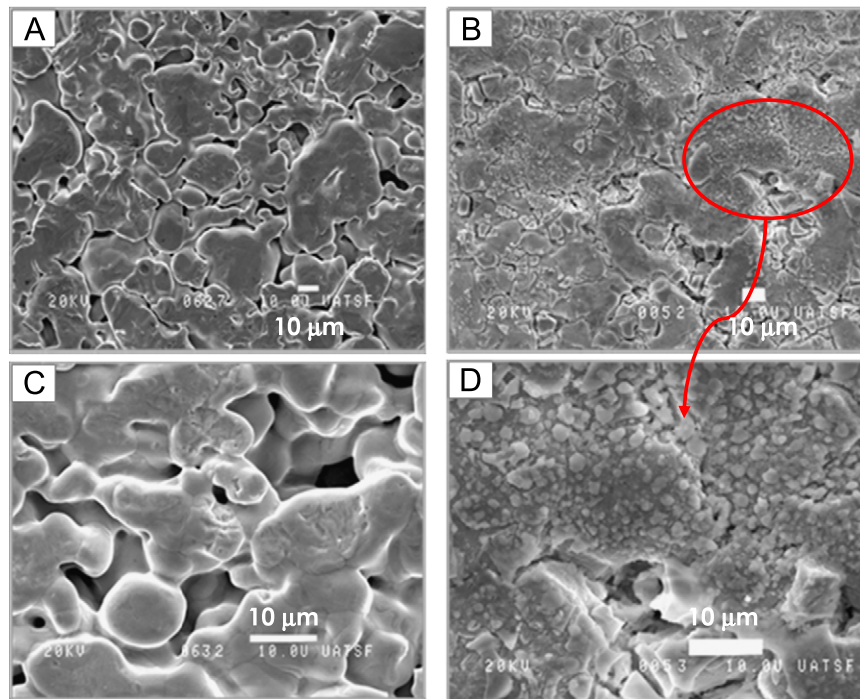
Fig. 3. SEM top view of the 0.2 μm support: (A) and (C) after oxidation; (B) and (D) after ZrO_2 coating followed by calcination up to 500 °C.
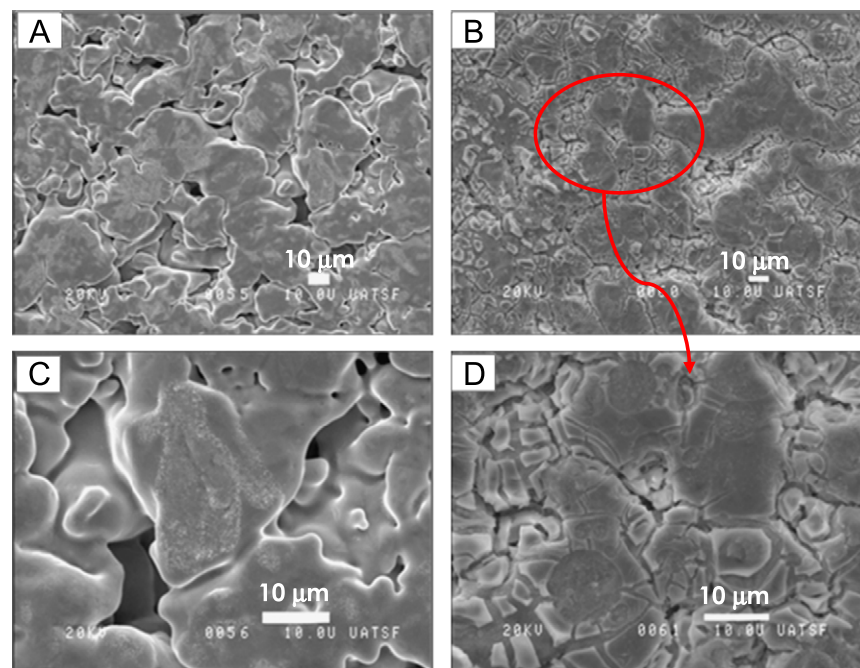

Fig. 4. SEM top view of the 0.1 μm support: (A) and (C) after oxidation; (B) and (D) after ZrO_2 coating followed by calcination up to 500 °C.

Table 2
Surface composition (at%) of the oxidized and ZrO_2-modified substrates.

	Surface composition (at%)				Binding energy (eV)			
	Fe	Cr	Zr	O	Fe 2p$_{3/2}$	Cr 2p$_{3/2}$	Zr 3d$_{5/2}$	O 1s
Oxidized PSSD	20.9	12.3	–	66.8	710.1	577.1	–	529.2
ZrO_2PSS0.2	nd[a]	nd	39.5	60.5	–	–	182.2	530.4

[a] nd: Not detected.

PdAuZrO$_2$0.2 membrane (Fig. 6C and D) becomes smoother in comparison with the PdAuAl$_2$O$_3$0.2, which may be due to the higher coverage of the support pores by the ZrO_2 coating. It is known that the microstructure of a Pd-based alloy film depends on a number of factors, such as substrate surface roughness and pore dimension. The reduced pore size in the ZrO_2-modified support enables the Pd-alloy layer to fill the pores more quickly and a thinner membrane layer could be obtained. As shown in Fig.7D and E, the metallic deposition starts to occur mainly

around the gaps formed on the ZrO_2 thin layer. This indicates that the PdAu layers proceed deep within the gaps before emerging on the surface layer. These plugs grow in size until they coalesce and form a continuous and uniform film on the surface of the ZrO_2-modified support. From SEM–EDS analysis, it was observed that the pores of the support were filled by ZrO_2. In addition, from the EDS cross-section line scan results (Fig. 7D–F), a thickness of the ZrO_2 layer lower than 1 µm could be inferred. On the other hand, in the Al_2O_3-modified support the pores were not completely filled by Al_2O_3 (Fig. 7A and B). The short Pd deposition performed during the support modification stage produced a thin Pd layer on the pores of the support which can be seen as a Pd-rich region in Fig. 7B. After this modification, the Pd and Au layers grew on top filling first the pore of the substrate and then forming a continuous layer (Fig. 7 A).

As it can be noticed in Fig. 7A, the PdAu thickness observed by SEM for the $PdAuAl_2O_30.2$ membrane was about 24 µm. It was found that the minimum thickness of PdAu alloy required for a gas-tightness membrane was about 20 µm when an Al_2O_3-modified support was employed. However, in the case of the ZrO_2-modified supports, half this thickness was required, close to 10 µm. By EDS cross-section line scan (Fig. 7C and F), both membranes showed a homogeneous composition in thickness of about Au 8–9%, displaying a uniform alloy formation. Neither Fe nor Cr was detected on the metallic layer of the $PdAuZrO_20.2$ membrane (Fig. 7F), showing that the modifier used is a good diffusion barrier. On the other hand, for the $PdAuAl_2O_30.2$ composite a 4–5% of Fe was detected on the support-Pd alloy inter-phase, showing that a slight inter-diffusion between the porous stainless steel component and the PdAu layer occurred.

Thus, we observed that the use of vacuum-assisted ZrO_2-modified porous stainless steel substrates allowed us to reduce the membrane film thickness and to avoid inter-metallic diffusion between the support and the palladium alloy layer.

Regarding the use of non-commercial ZrO_2-modified supports, Gao et al. [17] use a sol–gel derived zirconia procedure to obtain a thin layer on top of a porous stainless steel support. More recently, Zhang et al. [15] reported the use of a sol–gel derived mesoporous yttria stabilized zirconia layer as an intermediate layer to prevent inter-metallic diffusion on Pd membranes. The minimum Pd membrane thickness required for gas-tightness was 11 µm on top of a 3 µm YSZ/PSS support. Recently, Sanz et al. [9] reported the synthesis of a Pd membrane on top of an yttria-stabilized zirconia modified porous stainless steel tubular
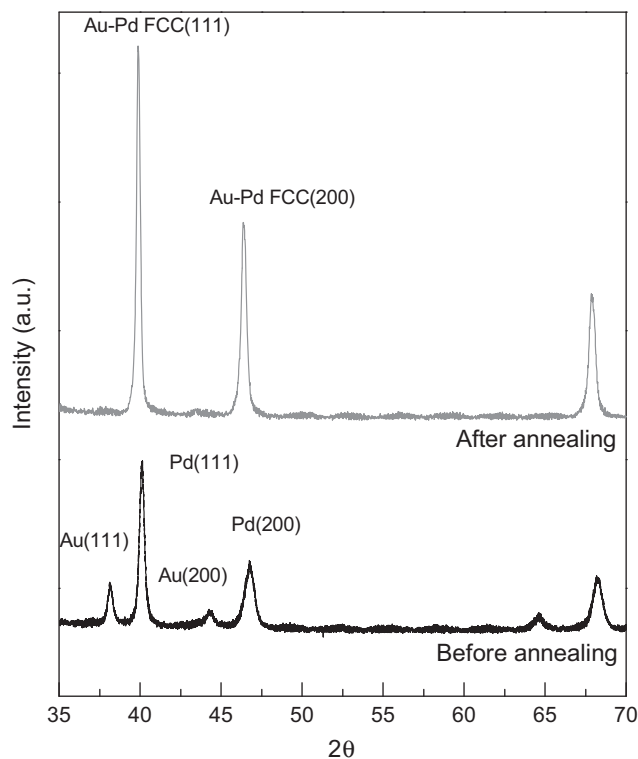
Table 3
XPS binding energies of the samples after permeation measurements.

Sample	BE (eV)		FWHM (eV)	
	Pd $3d_{3/2}$	Au $4f_{7/2}$	Pd $3d_{3/2}$	Au $4f_{7/2}$
$PdAuAl_2O_30.2$	340.4	83.6	1.20	0.96
$PdAuZrO_20.2$	340.5	83.7	1.19	1.00
$PdAuZrO_20.1$	340.6	83.6	1.18	0.99
Pd[a]	340.5	–	1.21	–
Au[b]	–	84.0	–	–

[a] Reference [21].
[b] Reference sample prepared by electroless plating.

Fig. 5. X-ray diffraction patterns of the $PdAuZrO_20.2$ membrane.

Table 4
Hydrogen permeation properties of several PdAu reported in the literature and those studied in this work.

Membrane	Au [at%]	Thickness [µm]	Temperature [ºC]	Permeability [mol s^{-1} m m^{-2} Pa$^{-0.5}$]	Selectivity H_2/N_2	Reference
PdAu/ceramic tube	6	3	400	1.3×10^{-8}	1,050	[20]
PdAu/ceramic tube	8	3	450	1.2×10^{-8}	1,400	[24]
$PdAu/Al_2O_3PSS$ disk	8	16	500	4.7×10^{-9}	142	[11]
PdAu/YSZ–PSS tube	5	2.3	400	1.3×10^{-8}	82,000	[8]
PdAu[a]	5.6 (10)[c]	25	450	1.5×10^{-8}	∞	[27]
PdAu[a]	12(20)[c]	25	450	1.4×10^{-8}	∞	[27]
$PdAuAl_2O_30.2$	8[d]	24[e]	400	7.8×10^{-9}	> 10,000	[This work]
$PdAuZrO_20.2$	9[d]	12[e]	400–450	1.1×10^{-8} to 1.5×10^{-8}	> 10,000	[This work]
$PdAuZrO_20.1$	8[d]	10[f]	400–450	9.9×10^{-9} to 1.3×10^{-8}	> 10,000	[This work]
$PdAuZrO_20.1$-1[b]	9[d]	11[f]	400–450	9.7×10^{-9} to 1.2×10^{-8}	> 10,000	[This work]
$PdAl_2O_3$ 0.2 PSS tube	-	22[e,f]	450	1.5×10^{-8}	200	[14]

[a] Self-supported membranes.
[b] Sample prepared with the same stages than $PdAuZrO_20.1$ membrane.
[c] wt%. Au composition is given between parenthesis.
[d] Determined by EDS.
[e] Determined by SEM.
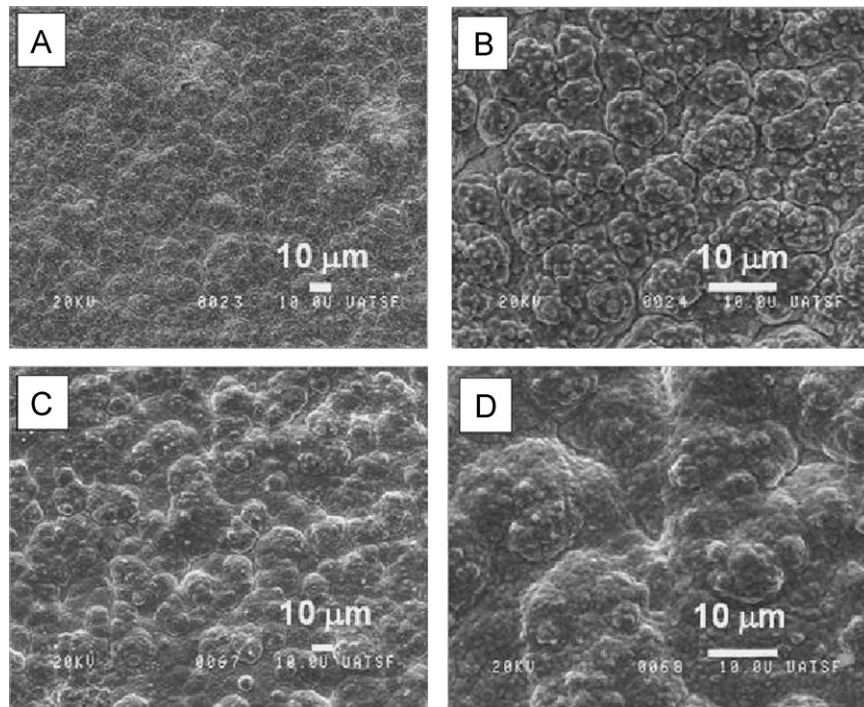[f] Determined gravimetrically.

Fig. 6. SEM top view of the PdAuAl$_2$O$_3$0.2 (A and B) and PdAuZrO$_2$0.2 (C and D) samples after hydrogen permeation experiments.
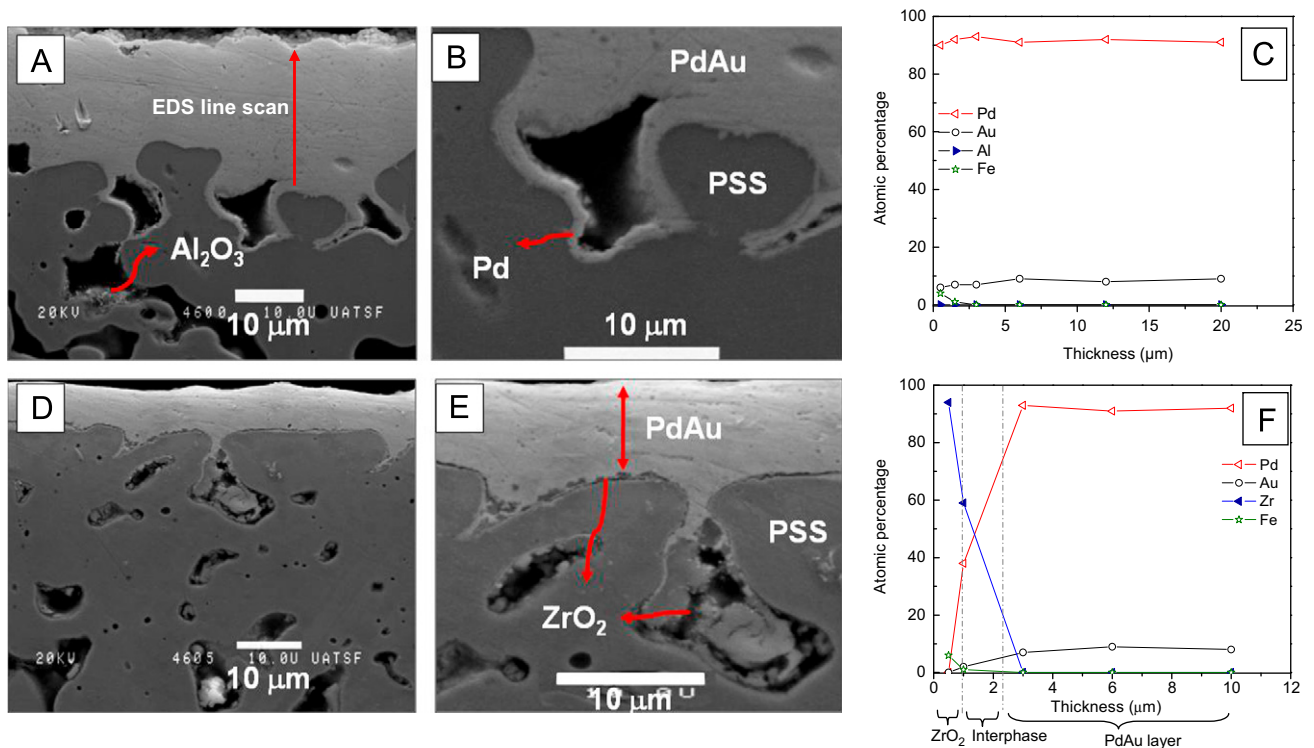

Fig. 7. SEM cross-section view of the PdAuAl$_2$O$_3$0.2 (A and B) and PdAuZrO$_2$0.2 (D and E) samples after hydrogen permeation experiments. EDS measurements along line on the films for PdAuAl$_2$O$_3$0.2 (D) and PdAuZrO$_2$0.2 (F) The PdAu layer and the ZrO$_2$ and Al$_2$O$_3$ coating are shown in the picture.

support. The YSZ layer of about 50 μm thickness was prepared by Atmospheric Plasma Spraying and the palladium membrane by electroless deposition. They reported that to achieve a dense and defect-free membrane a thickness of 27.7 μm of Pd layer was necessary.

The surface alloy formation was studied by means of XPS (Table 3). The membrane surface after the hydrogen permeation experiments was studied from the position of the Pd 3d$_{3/2}$, and Au 4f$_{7/2}$ core levels. The Pd 3d$_{5/2}$ signal is almost coincident with the Au 4d$_{5/2}$, so that the Pd 3d$_{3/2}$ was used. Gaussian–Lorentzian product GL(p) line shapes modified by an asymmetric form were used for fitting the spectra. The binding energy (BE) and the full weight at half maximum (FWHM) of the Pd 3d$_{3/2}$ and Au 4f$_{7/2}$ peaks are shown in Table 3. Note that the Au 4f$_{7/2}$ binding energy

shifts to a lower binding energy with respect to that reported for pure metallic gold [21]. This core-level binding energy shift could be assigned to the alloy formation. Besides, the Pd $3d_{3/2}$ binding energy did not present a significant modification with respect to pure Pd (Table 3). A chemical shift to lower binding energy under alloy formation has also been reported by other groups [22,23]. According to Hufner et al. [22], a shift of 0.7 to lower binding energy was observed for a $Pd_{90}Au_{10}$ alloy. On the other hand, Goodman and coworkers [23] reported that upon annealing up to 527 °C the Au $4f_{7/2}$ and Pd $3d_{3/2}$ peaks shift to lower binding energy by about 0.45 eV and 0.15 eV, respectively, which is in complete agreement with the data observed in our samples.

3.3. Permeation behavior of the synthesized membranes

The permeation behavior of the membranes was studied at several temperatures between 350 and 450 °C, with pressure differences between 10 and 100 kPa, after annealing at 500 °C in hydrogen stream during 120 h. Fig. 8A presents the hydrogen permeation flux through the PdAuZrO$_2$0.2 membrane as a function of the trans-membrane hydrogen pressures at different temperatures within 350 and 450 °C. The hydrogen flux obeys Sieverts' law in the entire temperature range studied. This trend is consistent with the solution–diffusion mechanism of pure hydrogen through a palladium-alloy membrane, when the rate determining step was the diffusion of H in the metallic alloy bulk film. At 450 °C and 100 kPa, this membrane presented a single component H_2 flux of ca. 0.16 mol s^{-1} m^{-2} and a H_2/N_2 ideal selectivity higher than 10,000 (Fig. 8A). When a sweep gas flow was employed with a diferential pressure of 100 kPa, the N_2 flow rate was below the minimum detection limit of the mass spectrometer used to check the N_2 leak.

The single component hydrogen permeation fluxes as a function of the trans-membrane pressure for all the synthesized membranes are shown in Fig. 8B at 400 °C. Note that the fluxes of the ZrO$_2$-modified membranes are about 3.5 higher than those of the PdAuAl$_2$O$_3$0.2 membrane, which is consistent with the lower thickness of the PdAu layer. All the membranes exhibited no-detectable nitrogen permeation flux over the range of pressure tested, confirming that the PdAu membranes synthesized were almost pinhole-free. These data show that a better performance on hydrogen

permeation could be reached if the the ZrO$_2$-modified supports prepared in this work were used under the same experimental conditions.

A comparison between our permeation data and those reported in the literature for PdAu membranes with similar gold concentration is presented in Table 4. A rigorous comparison with the literature data is, however, difficult since factors such as membrane preparation and thickness have a direct effect on the permeation properties. As is well known, permeability should be independent of thickness, as long as bulk diffusion is the rate-controlling step. Therefore, the H_2 permeability of the membranes is also included in Table 4. The H_2 permeabilities of the PdAu alloys synthesized on top of the vacuum-assisted ZrO$_2$-modified supports (ca. 1.5×10^{-8} mol s^{-1} m m^{-2} Pa$^{-0.5}$) were similar to the best data reported in the literature for PdAu self-supported membranes and PdAu ceramic membranes. For PdAu nano-layered membranes synthesized on top of porous ceramic tubes, Goldbach and coworkers [24] reported a permeability of about 1.2×10^{-8} mol s^{-1} m m^{-2} Pa$^{-0.5}$. On the other hand, Way and coworkers [8] synthesized a 2.3 μm thick Pd$_{95}$Au$_5$ membrane on top of a commercially available YSZ-modified PSS tube. At 400 °C and a differential pressure of 138 kPa, they reported a pure H_2 permeation flux of about 1.01 mol s^{-1} m^{-2}, a H_2/N_2 ideal selectivity over 80,000 and a permeability of ca. 1.36×10^{-8} mol s^{-1} m m^{-2} Pa$^{-0.5}$. This value was similar to the data obtained with our PdAu composites, showing the good performance of our membranes. Notice that the measured relative permeability normalized with respect to pure Pd for the PdAuZrO$_2$0.2 was about 1, when the gold composition was close to 9 atomic %.

In the case of the PdAuAl$_2$O$_3$0.2 membrane, the hydrogen permeability was about 0.7 times the permeability of the PdAu ZrO$_2$-modified membranes. A significant loss in hydrogen permeability at temperatures higher than 615 °C as a result of the diffusion of Al into the Pd alloy layer has been reported for Pd and PdAg alloy membranes synthesized on top of α-Al$_2$O$_3$ substrates by Okazaki et al. [25,26]. These authors claimed that the atomic hydrogen presented at the interface between the α-Al$_2$O$_3$ and the Pd layer induced the reduction of Al$_2$O$_3$ to Al and produced the migration of Al into the Pd layer. It should be noticed that the temperature at which the decline in hydrogen permeation was observed is higher than the temperature of exposure of our membranes (500 °C). From the SEM-EDS cross-section data of the
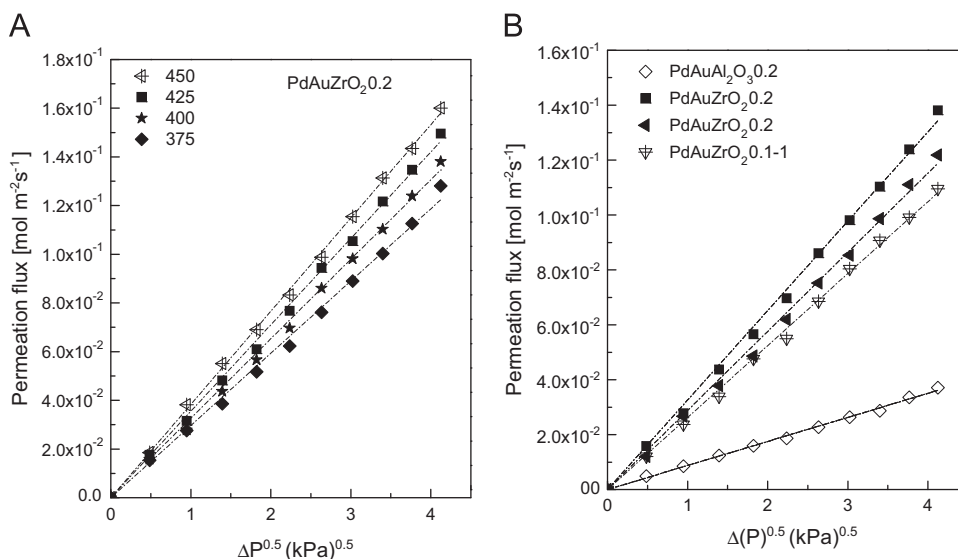

Fig. 8. Sieverts' plot of the membranes: (A) hydrogen flux at different temperatures for the PdAuZrO$_2$0.2 membrane; (B) hydrogen flux for the three membranes at 400 °C as a function of the pressure difference across the membranes.
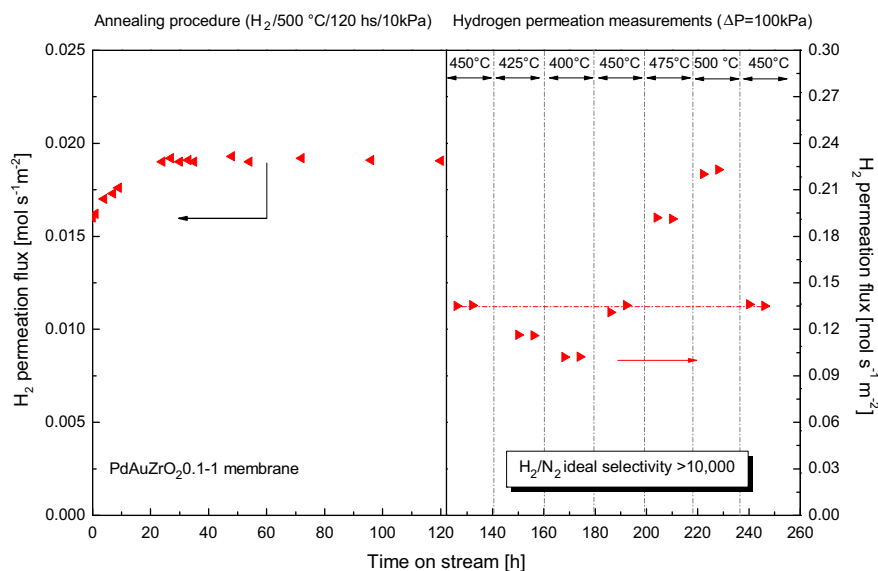
Fig. 9. Thermal stability and permeation history of the PdAuZrO$_2$0.1-1 membrane.

PdAuAl$_2$O$_3$0.2 membrane, aluminum was not observed into the Pd alloy layer; therefore, we could not confirm the formation of PdAl alloys upon hydrogen permeation experiments. However, a slight inter-diffusion between the porous stainless steel component and the PdAu layer was observed, and 4–5% of Fe was detected on the support-Pd alloy inter-phase through EDS. On the other hand, the resistance of the support could influence the permeation flux of the composite membranes. Nevertheless, as stated above, the PdAuZrO$_2$ membranes synthesized in this work, exhibit H$_2$ permeabilities similar to those reported for PdAu self-supported and PdAu ceramic membranes.

In order to verify the thermal stability of the PdAuZrO$_2$-modified membranes, a new sample (PdAuZrO$_2$0.1-1) was prepared employing the same preparation stages than the PdAuZrO$_2$0.1. This membrane was subjected to a difference cycle of permeation experiments. The sample was first annealed up to 500 °C in H$_2$ flux during 120 h in order to form a uniform PdAu alloy layer in the same way as the other membranes. During this period, the H$_2$ permeation flux was measured as a function of annealing time. For this membrane, the hydrogen permeation rate became stable within 30 h at 1.9 $\times 10^{-1}$ mol s^{-1} m^{-2} (Fig. 9). After the total annealing time, it was cooled down to 450 °C and the H$_2$ permeation flux was obtained as a function of the trans-membrane pressure at different temperatures. Once the permeation properties were evaluated at 450 °C, 425 °C and 400 °C, the membrane was heated up to 450 °C again to check the stability and reproducibility of the H$_2$ flux. It should be noted that the permeation properties of the membrane at 450 °C did not present any significant variation after 50 h (about 190 h on stream). Then, the H$_2$ flux was measured at higher temperatures, 475 °C and 500 °C, and the membrane was cooled down again up to 450 °C. It is important to notice that no significant modification in the permeation flux was observed even after heating up to 500 °C. During the experiments, the membrane was systematically checked for leakages, showing that the PdAu composite remained with a high H$_2$/N$_2$ selectivity (> 10,000) even after about 250 h on stream.

4. Conclusions

It was shown that the use of vacuum-assisted ZrO$_2$-modified PSS supports allows the obtention of defect free PdAu membranes with good performance and significantly lower thickness than those obtained under the same conditions on top of alumina-modified PSS supports.

SEM cross-section results showed that dense, continuous, defect-free PdAu films were deposited on top of the ZrO$_2$-modified PSS disks, and the EDS line scan data indicated that no significant composition gradient was present on the thickness after hydrogen permeation experiments.

All PdAuZrO$_2$ membranes studied showed a good performance, with hydrogen permeabilities of ca. 1.5×10^{-8} mol s^{-1} m m^{-2} Pa$^{-0.5}$, similar to the best data reported in the literature and high H$_2$/N$_2$ ideal selectivity (> 10,000). The PdAuZrO$_2$0.1-1 composite membrane was stable for at least 250 h in hydrogen stream upon heating up to 500 °C.

References

[1] M.E. Ayturk, E.E. Engwall, Y.H. Ma, Microstructure analysis of the intermetallic diffusion-induced alloy phases in composite Pd/Ag/porous stainless steel membranes, Ind. Eng. Chem. Res 46 (2007) 4295.
[2] Y.-H. Chi, P.-S. Yen, M.-S. Jeng, S.-T. Ko, T-C. Lee, Preparation of thin Pd membrane on porous stainless steel tubes modified by a two-step method, Int. J. Hydrog. Energy 35 (2010) 6303.
[3] C. Su, T. Jin, K. Kuraoka, Y. Matsumura, T. Yazawa, Thin palladium film supported on SiO$_2$-modified porous stainless steel for a high-hydrogen-flux membrane, Ind. Eng. Chem. Res. 44 (2005) 3053.
[4] J. Tonga, C. Sua, K. Kuraoka, H. Suda, Y. Matsumura, Preparation of thin Pd membrane on CeO$_2$-modified porous metal by a combined method of electroless plating and chemical vapor deposition, J. Membr. Sci 269 (2006) 101.
[5] M. Zahedi, B. Afra, M. Dehghani-Mobarake, M. Bahmani, Preparation of a Pd membrane on a WO$_3$modified porous stainless steel for hydrogen separation, J. Membr. Sci 333 (2009) 45.
[6] M.L. Bosko, F. Ojeda, E.A. Lombardo, L.M. Cornaglia, NaA zeolite as an effective diffusion barrier in composite Pd/PSS membranes, J. Membr. Sci 331 (2009) 57.
[7] Y.H. Ma, B.C. Akis, M.E. Ayturk, F. Guazzone, E.E. Engwall, I.P. Mardilovich, Characterization of intermetallic diffusion barrier and alloy formation for Pd/Cu and Pd/Ag porous stainless steel composite membranes, Ind. Eng. Chem. Res 43 (2004) 2936.

[8] Ø. Hatlevik, S.K. Gade, M.K. Keeling, P.M. Thoen, A.P. Davidson, J.D. Way, Palladium and palladium alloy membranes for hydrogen separation and production: history, fabrication strategies, and current performance, Sep. Purif. Technol. 73 (2010) 59.

[9] R. Sanz, J.A. Calles, D. Alique, L. Furones, S. Ordóñez, P. Marín, P. Corengia, E. Fernandez, Preparation, testing and modelling of a hydrogen selective Pd/YSZ/SS composite membrane, Int. J. Hydrog. Energy (2011) 15783.

[10] J.D., Way, M. Lusk, P. Thoen, Sulfur-resistant composite metal membranes, US Patent 8,101,243 B2.

[11] Ch-H. Chen, Y.H. Ma, The effect of H$_2$S on the performance of Pd and Pd/Au composite membrane, J. Membr. Sci 362 (2010) 535.

[12] S.K. Gade, E.A. Payzant, H.J. Park, P.M. Thoen, J.D. Way, The effects of fabrication and annealing on the structure and hydrogen permeation of Pd–Au binary alloy membranes, J. Membr. Sci 340 (2009) 227–233.

[13] M.L. Bosko, J.B. Miller, E.A. Lombardo, A.J. Gellman, L.M. Cornaglia, Surface characterization of Pd–Ag composite membranes after annealing at various temperatures, J. Membr. Sci 369 (2011) 267.

[14] A.M. Tarditi, F. Braun, L.M. Cornaglia, Novel PdAgCu ternary alloy: hydrogen permeation and surface properties, Appl. Surf. Sci. 257 (2011) 6626.

[15] K. Zhang, H. Gao, Z. Rui, P. Liu, Y. Li, Y.S. Lin, High-temperature stability of palladium membranes on porous metal supports with different intermediate layers, Ind. Eng. Chem. Res. 48 (2009) 1880.

[16] S.-M. Chang, R.D. Doong, Chemical-composition-dependent metastability of tetragonal ZrO2 in sol-gel-derived films under different calcination conditions, Chem. Mater. 17 (2005) 4837.

[17] H. Gao, Y. Li, J.Y.S. Lin, B. Zhang, Characterization of zirconia modified porous stainless steel supports for Pd membranes, J. Porous. Mater 13 (2006) 419.

[18] I.P. Mardilovich, E. Engwall, Y.H. Ma, Dependence of hydrogen flux on the pore size and plating surface topology of asymmetric Pd-porous stainless steel membranes, Desalination 144 (2002) 85.

[19] H. Xu, D.-H. Qin, Z. Yang, H.-L. Li, Fabrication and characterization of highly ordered zirconia nanowire arrays by sol–gel template method, Mater. Chem. Phys 80 (2003) 524.

[20] L. Shi, A. Goldbach, G. Zeng, H. Xu, Preparation and performance of thin-layered PdAu/ceramic composite membranes, Int. J. Hydrog. Energy 35 (2010) 4201.

[21] K. Asami, A precisely consistent energy calibration method for X-ray photo-electron spectroscopy, J. Electron. Spectrosc 9 (1976) 469.

[22] S. Hüfner, G.K. Wertheim, J.H. Wernick, XPS core line asymmetries in metals, Solid. State. Commun. 17 (1975) 417.

[23] C.-W. Yi, K. Luo, T. Wei, D.W. Goodman, The composition and structure of Pd−Au surfaces, J. Phys. Chem. B. 109 (2005) 18535.

[24] L. Shi, A. Goldbach, H. Xu, High-flux H$_2$ separation membranes from (Pd/Au)$_n$ nanolayers, Int. J Hydrog. Energy 36 (2011) 2281.

[25] J. Okazaki, T. Ikeda, D.A. Pacheco Tanaka, K. Sato, T.M. Suzuki, F. Mizukami, An investigation of thermal stability of thin palladium–silver alloy membranes for high temperature hydrogen separation, J. Membr. Sci 366 (2011) 212.

[26] J. Okazaki, T. Ikeda, D.A. Pacheco Tanaka, M.A. Llosa Tanco, Y. Wakui, K. Sato, F. Mizukami, T. Suzuki, Importance of the support material in thin palladium composite membranes for steady hydrogen permeation at elevated temperatures, Phys. Chem. Chem. Phys. 11 (2009) 8632.

[27] S.K. Gade, K.E. Coulter, J.D. Way, Effects of fabrication technique upon material properties and permeation characteristics of palladium–gold alloy membranes for hydrogen separations, Gold Bull. 43 (2010) 287–297.